Adsorption Rate Constants from Chromatography

P. SCHNEIDER and J. M. SMITH

University of California, Davis, California

A new method for determining adsorption equilibrium constants, rate constants, and intraparticle diffusivities is described and applied for the adsorption of ethane, propane, and *n*-butane on silica gel. The method rests upon recently developed theory for relating the moments of the effluent concentration wave from a bed of adsorbent particles to the rate constants associated with the various steps in the overall adsorption process. It is necessary to operate at concentrations of adsorbable gas such that the adsorption isotherm is linear. However, it is possible to take into account effects of longitudinal dispersion and diffusion to the particle surface as well as the intraparticle processes of diffusion and adsorption on the pore surface.

The method gave reasonable values for intraparticle diffusivities and adsorption rate constants. Intraparticle diffusion was a major resistance for all particle sizes studied and for the largest size (R = 0.50 mm.) this step controlled the overall rate.

From the consrants determined chromatographically it is possible to predict breakthrough curves for the adsorption of these hydrocarbons on silica gel. The predicted curves agree well with experimentally established breakthrough curves.

The importance of separating gases by fluid-solid operations has created a need for predicting the performance of adsorption equipment. The design of fixed-bed adsorbers particularly involves the prediction of the concentration-time relationship, or breakthrough curve, of the effluent stream. Apart from the influence of axial dispersion, a mathematical model of adsorption from the gas stream should take into account: (a) diffusion of the component from the main body of the gas phase to the external surface of the adsorbent particle (external diffusion), (b) diffusion through the porous network of the particle (internal diffusion), and (c) the adsorption process itself. Quantitative treatment of rates of adsorption using this model requires values of the diffusion and adsorption rate constants that describe the three steps. The purpose of this study is to show that such constants, as well as axial diffusivities, can be evaluated from relatively simple chromatographic measurements. The overall validity of the methods can be ascertained by comparing breakthrough curves measured experimentally with those predicted from the rate constants.

P. Schneider is on leave from the Institute of Chemical Process Fundamentals, Czechoslovak Academy of Sciences, Prague, Czechoslovakia.

THEORY

The concentration, $c(z, t)$, of the adsorbing gas as a function of time and axial position in the bed can be obtained by solving the following system of equations:
mass balance of the adsorbable component in the gas phase:

$$\frac{E_A}{\alpha}\frac{\partial^2 c}{\partial z^2} - v\frac{\partial c}{\partial z} - \frac{\partial c}{\partial t} - \frac{3D_c}{R}\frac{1-\alpha}{\alpha}\left(\frac{\partial c_i}{\partial r}\right)_{r=R} = 0 \quad (1)$$

mass balance of this component in the particle

$$\frac{D_c}{\beta}\left(\frac{\partial^2 c_i}{\partial r^2} + \frac{2}{r}\frac{\partial c_i}{\partial r}\right) - \frac{\partial c_i}{\partial t} - \frac{\rho_p}{\beta}\frac{\partial c_{\text{ads}}}{\partial t} = 0 \quad (2)$$

rate of adsorption (assumed to be linear)

$$\frac{\partial c_{\text{ads}}}{\partial t} = k_{\text{ads}}\,(c_i - c_{\text{ads}}/K_A) \quad (3)$$

external diffusion boundary condition

$$D_c\left(\frac{\partial c_i}{\partial r}\right)_{r=R} = k_f\,(c - c_i) \quad (4)$$

internal diffusion boundary condition

$$\frac{\partial c_i}{\partial r} = 0 \quad \text{at} \quad r = 0 \quad \text{for} \quad t > 0 \tag{5}$$

and the initial conditions

$$c = 0, \quad \text{at} \quad z > 0 \quad \text{for} \quad t = 0 \tag{6}$$

$$c_i = 0, \quad \text{at} \quad r \geq 0 \quad \text{for} \quad t = 0 \tag{7}$$

Conditions (6) and (7) state that the adsorbent does not contain any adsorbed species at the start of the run. Then condition (8) specifies that at the bed inlet the concentration of the adsorbable species is maintained constant, thus

$$c = c_o \quad \text{at} \quad z = 0 \quad \text{for} \quad t > 0 \tag{8}$$

Recently Masamune and Smith (*1, 2*) have solved this problem when axial dispersion plays no role ($E_A = 0$) and when the equilibrium adsorption isotherm is linear (Henry's region). They used the mathematical method first developed by Rosen (*3*) for the case when only intraparticle diffusion is significant. The solution is expressed in terms of an infinite integral which must be evaluated numerically:

$$\frac{c(z,t)}{c_o} = (1/2) + (2/\pi)\int_o^\infty (1/y) \exp[A_1(y)] \sin[A_2(y)]dy \tag{9}$$

$$A_1(y) = -3\,\mathbf{D}[\omega_1 + \mathbf{E}(\omega_1^2 + \omega_2^2)]/[(1 + \mathbf{E}\,\omega_1)^2 + (\mathbf{E}\,\omega_2)^2] \tag{10}$$

$$A_2(y) = \mathbf{D}\{\mathbf{A}\tau y^2 - [3\omega_2/[(1 + \mathbf{E}\,\omega_1)^2 + (\mathbf{E}\,\omega_2)^2]]\} \tag{11}$$

$$\omega_1 = [\phi_1 \sin(2\phi_1) + \phi_2 \sinh(2\phi_2)]/[\cosh(2\phi_2) - \cos(2\phi_1)] - 1 \tag{12}$$

$$\omega_2 = [\phi_2 \sin(2\phi_1) + \phi_1 \sinh(2\phi_2)]/[\cosh(2\phi_2) - \cos(2\phi_1)] \tag{13}$$

$$\phi_1 = -\sqrt{\mathbf{A}\,y^2/[2(y^4 + 1)(\sqrt{y^4 + 1} + y^2)]} \tag{14}$$

$$\phi_2 = \sqrt{\mathbf{A}y^2/[2(y^4 + 1)(\sqrt{y^4 + 1} - y^2)]} \tag{15}$$

In these equations τ is a normalized time

$$\tau = t/t_o \tag{16}$$

where t_o is the time necessary for saturation of the adsorbent under conditions where there is no resistance at all. It is given by

$$t_o = \frac{1-\alpha}{\alpha} \rho_p K_A \frac{z}{v} \tag{17}$$

The dimensionless parameters **D**, **E**, and **A** [Equations (18) to (20)] are defined as follows:

$$\mathbf{D} = \frac{D_c}{R^2} \frac{1-\alpha}{\alpha} \frac{z}{v} \tag{18}$$

$$\mathbf{E} = \frac{D_c}{k_f R} \tag{19}$$

$$\mathbf{A} = \frac{R^2}{D_c} k_{ads} \rho_p \tag{20}$$

They contain the rate constants which describe external diffusion, internal diffusion, and adsorption rate, and are therefore characteristics of these processes.

When the rate constants D_c, k_f and k_{ads} are known, it is possible to calculate by means of Equations (9) to (20) the $c = c(t,z = \text{const.})$ curve, point by point, for an adsorber bed characterized by the values of z, α, ρ_p, R, and for a specific value of the gas velocity, v. However, the values of the constants are rarely known. In fact the usual procedure of finding them consists of comparing experimental breakthrough curves obtained in a small adsorber with curves predicted from Equations (9) to (20). Such a procedure is not very satisfactory because more than one set of the three constants can usually be found which give a curve in good agreement with the experimental data. What is needed is an independent method of finding these constants by using a simple experimental and evaluation technique.

Recently there have appeared papers (*4* to *6*) which greatly improved the theoretical treatment of gas-solid chromatography. The Kubin and Kucera theory appears to be more general than the earlier work of van Deemter and Zuiderweg, and the equations of the earlier theories can be developed as special cases of the Kubin and Kucera theory. The set of differential equations which describe the movement of an adsorbable substance in a chromatographic column is identical with the set for an adsorber, that is, Equations (1) to (7). The only difference in the two cases is the bed-inlet condition. Instead of Equation (8), the pulse input can be described by the square function (*4,5*)

$$c = c_o \text{ at } z = 0 \text{ for } 0 \leq t \leq t_{oA}$$

$$c = 0 \text{ at } z = 0 \text{ for } t > t_{oA} \tag{21}$$

where t_{oA} is the injection time of the adsorbable gas of concentration c_o. By using the Laplace-Carson transform as defined by Equation (22) we obtain

$$s(z,p) = p\int_0^\infty c(z,t) \exp(-pt)dt, \tag{22}$$

Kubin (*5*) solved the system of Equations (1) to (7) and (21), and obtained for the transform, $s(z,p)$, of the concentration function, $c(z,t)$, the expression

$$s(z,p) = c_o[1 - \exp(-pt_{oA})] \exp(-\gamma z) \tag{23}$$

where

$$\gamma = -\frac{v\alpha}{2E_A} + \sqrt{\left(\frac{v\alpha}{2E_A}\right)^2 + \frac{p\alpha}{E_A}[1 + h(p)]} \tag{24}$$

and

$$h(p) = \frac{3k_f}{R} \frac{1-\alpha}{\alpha} \left\{ \frac{1}{p} - \frac{\sinh(R\sqrt{\lambda})}{(pD_c/k_f)\sqrt{\lambda}\cosh(R\sqrt{\lambda}) + p[1 - (D_c/Rk_f)]\sinh(R\sqrt{\lambda})} \right\} \tag{25}$$

$$\lambda = \frac{p\beta}{D_c}\left[1 + \frac{(\rho_p/\beta)K_A k_{ads}}{K_A p + k_{ads}}\right] \tag{26}$$

Though it does not appear feasible to invert the transform, it is possible to obtain directly from $s(z,p)$, explicit expressions for the moments of the chromatographic curve, $c(z,t)$.

The nth absolute moment, μ'_n, of the function, $c(z,t)$, is defined as

$$\mu'_n = m_n/m_o \tag{27}$$

where

$$m_n = \int_0^\infty t^n\, c(z,t)\, dt \qquad (n = 0, 1, 2, 3, \ldots) \tag{28}$$

The nth central moment μ_n is defined as

$$\mu_n = (1/m_0)\int_0^\infty (t-\mu'_1)^n\, c(z,t)\, dt \tag{29}$$

(The first absolute moment, μ'_1, characterizes the position of the center of gravity of the chromatographic curve, whereas the second central moment μ_2 depends on the width of this curve.) The evaluation of the moments (7) from a knowledge of $s(z,p)$ is based on

$$m_n = (-1)^n \lim_{p\to 0} \frac{d^n}{dp^n}\,[s(z,p)/p] \tag{30}$$

By using Equations (27) to (30) together with Equations (23) to (26) the first absolute, and second and third central, moments (μ'_1, μ_2, μ_3) can be expressed as follows:

$$\mu'_1 = (z/v)(1+\delta_0) + (t_{oA}/2) \tag{31}$$

$$\mu_2 = (2z/v)[\delta_1 + (E_A/\alpha)(1+\delta_0)^2(1/v^2)] + (t_{0A}^2/12) \tag{32}$$

$$\mu_3 = (3z/v)[\delta_2 + 4(E_A/\alpha)\delta_1(1+\delta_0)(1/v^2) + 4(E_A/\alpha)^2(1+\delta_0)^3(1/v^4)] \tag{33}$$

where

$$\delta_0 = [(1-\alpha)\beta/\alpha][1 + (\rho_p/\beta)K_A] \tag{34}$$

$$\delta_1 = [(1-\alpha)\beta/\alpha)]\left[\frac{\rho_p}{\beta}\frac{K_A^2}{k_{\text{ads}}} + \frac{R^2\beta}{15}\left(1+\frac{\rho_p}{\beta}K_A\right)^2\left(\frac{1}{D_c}+\frac{5}{k_fR}\right)\right] \tag{35}$$

$$\delta_2 = \lim_{p\to 0}\frac{d^2}{dp^2}\,[h(p)] \tag{36}$$

Experimental chromatographic curves of the effluent from the bed can be used in Equations (27) to (29) to evaluate the moments μ'_1 and μ_2. Data at different velocities and particle radii, R, will give the moments as a function of these two variables. Then Equations (31), (32), (34), and (35) can be used to evaluate the axial dispersion coefficient, E_A, intraparticle diffusion coefficient, D_c, adsorption rate constant, k_{ads}, mass tranfser coefficient, k_f, as well as the adsorption equilibrium constant, K_A. In this way all the constants necessary for the prediction of the breakthrough curve by means of Equations (9) to (20) are available. (The axial dispersion coefficient, E_A, is not used in these latter calculations, because the mathematical model of adsorber on which Equations (9) to (20) are based does not take into account axial dispersion).

In this study both chromatographic curves and breakthrough curves were measured experimentally. Rate constants were evaluated from the chromatographic curves and used to predict breakthrough curves. Agreement between the experimental and calculated curves should confirm the theory of gas-solid chromatography as well as the model used for the adsorber. Good agreement would also suggest that the rate constants determined by gas chromatography have physical significance and are not simply empirical constants.

EXPERIMENTAL

Breakthrough and chromatographic curves of ethane, propane, and n-butane, on silica gel at 50°C. and atmospheric pressure, were measured. Helium was used as the carrier gas and the concentrations of hydrocarbon were very low so that the assumption of the linear adsorption isotherm was fulfilled. This was tested by comparing K_A, determined chromatographically, with the value measured by the dynamic adsorption method. The injection of the square concentration function. Equation (21), was accomplished with a special sampling valve, rather than by injection of the sample with hypodermic syringe, which is frequently used. The three particle sizes of silica gel which were used covered a twentyfold range of R^2 (0.012-0.25 sq. mm.), the velocity of carrier gas ranged from 1.2 to 15 cm/sec.

Adsorbent

Silica gel of 6-16 mesh was fractured, ground, and separated by sieves. The sizes were chosen so that the average of the openings of two adjoining sieves differed from the dimension of the openings of these two sieves by 7 to 8%. This average opening was taken as the diameter of the equivalent spherical particle. For the equilibrium adsorption measurements particles of R = 0.04 mm. were used. In the other experiments fractions of R = 0.50, 0.39, and 0.11 mm. were utilized. The pretreatment of the adsorbent consisted of heating in the apparatus for 18 hr. at 200°C. in a stream of dry helium. The physical properties of the gel (8)were specific surface area 832 sq. m./g., void volume 0.43 ml./g., internal void fraction β = 0.486, particle density ρ_p = 1.13 g./ml. The average pore radius was 11 Å.

Gases

The helium of stated purity 99.99% was dried before use by passing it through a metal trap cooled by a dry ice-acetone mixture. To avoid the necessity of regulation and measurement of flow rates differing by two or three orders of magnitude, the hydrocarbons were used in the form of dilute mixtures with helium. These mixtures contained 4.0 vol. % ethane, or 4.0 vol. % propane, or 0.92 vol. % n-butane. Prior to adsorption these individual streams were mixed with additional pure helium and dried by passing through cooled (dry ice-acetone) traps.

Pure hydrocarbons were used for calibration purposes. These were chemically pure grade (purity > 99%) gases.

Equilibrium Adsorption Measurements

Equilibrium adsorption isotherms of the individual hydrocarbons were measured by the dynamic flow method in a Perkin-Elmer Shell Sorptometer. Figure 1 is a schematic drawing of the apparatus. The flow rates of pure helium and the helium-hydrocarbon mixture were maintained constant by automatic pressure regulators regulated by needle valves, and measured by calibrated capillary flowmeters. After mixing, these two streams passed through the cooled trap and entered the reference side of the thermal conductivity cell,

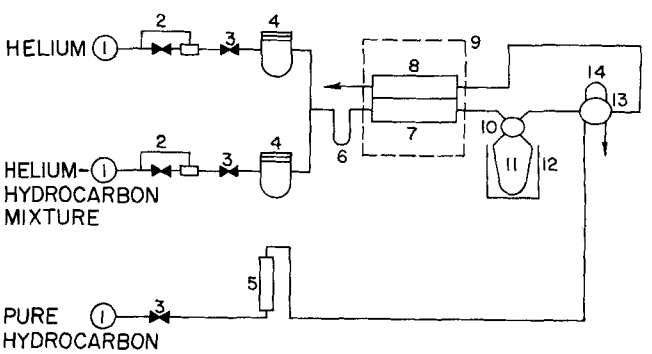

Fig. 1. Schematic diagram of the adsorption apparatus. 1. gas cylinder; 2. automatic pressure regulator; 3. needle valve; 4. capillary flowmeter; 5. rotameter; 6. cooling trap (dry ice-acetone mixture); 7. reference side, thermal conductivity cell; 8. sample side, thermal conductivity cell; 9. water bath; 10. four-way valve; 11. adsorber; 12. constant temperature bath; 13. six-way calibration valve; 14. calibration loop.

which was immersed in a constant temperature water bath. Leaving the cell the gases entered the adsorber via a four-way metal valve. The adsorber consisted of a U-tube, in one arm of which was the bed of adsorbent. During the adsorption run the adsorber was in a constant temperature water bath, in which the temperature was maintained at 50°C. (± 0.05°C.). For desorption the adsorber was immersed in an oil bath heated to 200°C. by means of the immersion heater. Leaving the adsorber, the gases passed through the sample side of the thermal conductivity cell, and then were discharged via a soap flowmeter. The sample loop with the six-way valve served for introducing into the gas stream a known amount of pure hydrocarbon (from cylinder via the regulation needle valve and rotameter).

During the run the gas mixture with a known context of hydrocarbon passed through the adsorber. When adsorption was completed (usually after 1 hr.) the four-way valve was turned so that the adsorber was disconnected from the flowing gas. The water bath was replaced by the heated oil bath and desorption proceeded at 200°C. (for about 15 min.). After turning the four-way valve the desorbed hydrocarbon was flushed from the adsorber into the sample side of the thermal conductivity cell by the gas stream. The amount of the desorbed hydrocarbon was determined by comparison of the areas of the desorption and calibration peaks. The latter was obtained by flushing with helium a known amount of pure hydrocarbon, contained in the calibration loop, through the conductivity cell.

The areas of the desorption and calibration peaks were measured by the Perkin-Elmer Printing Integrator (model 194B) and by weighing the cut-out peaks. The agreement of these two methods was within 1%.

Chromatographic and Breakthrough Measurements

Chromatographic and breakthrough curves were measured in the apparatus schematically sketched in Figure 2. This included a constant temperature gas chromatograph (Model 600-D, Varian Aerograph) with flame ionization detector. The ordinary chromatographic column was replaced by shorter columns which contained silica gel. A six-way, two-position sampling valve, built in the chromatograph, permitted injection of a step function in concentration (when the breakthrough curves were measured) as well as a square function (in following the chromatographic peaks). The left part of Figure 2 represents the setup for preparation of helium-hydrocarbon mixtures. In Figure 3 the two positions of the sampling valve are depicted together with the directions of the flowing gases. The outlet of the column was connected directly to the flame ionization detector. The short tubing which connected the sampling valve with the column inlet was 0.04 in. I.D. so

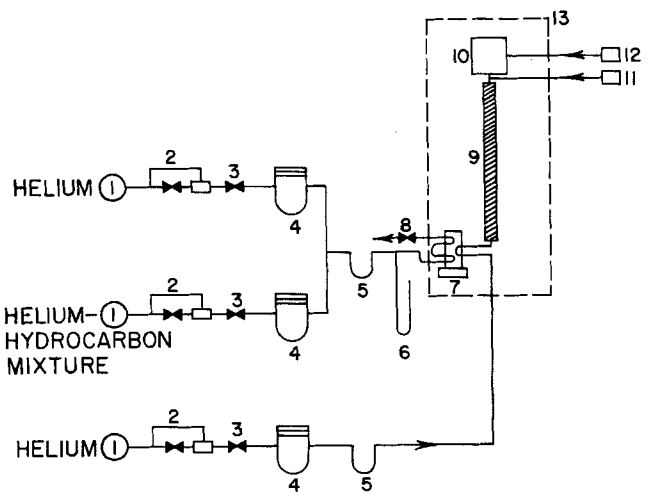

Fig. 2. Schematic diagram of the apparatus. 1. gas cylinder; 2. automatic pressure regulator; 3. regulation needle valve; 4. capillary flowmeter; 5. cooling trap (dry ice-acetone mixture); 6. mercury manometer; 7. two-position, six-way sampling valve (see also Figure 3); 8. needle valve; 9. column with adsorbent; 10. flame ionization detector; 11. electrolytic generator of hydrogen; 12. air pump; 13. chromatograph oven.

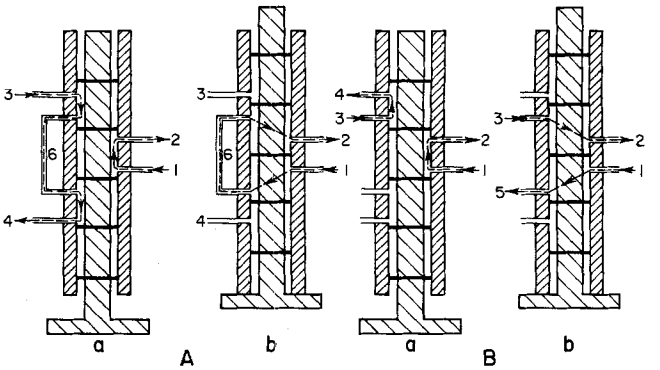

Fig. 3. Sampling valve. A. arrangement for chromatography, B. arrangement for breakthrough curves measurement; (a) normal position, (b) feeding position. 1. carrier gas (helium) inlet; 2. to the column; 3. hydrocarbon-helium mixture inlet; 4. hydrocarbon-helium mixture outlet; 5. carrier gas outlet; 6. sample loop.

that the holdup volume in the apparatus was very small.

When the chromatographic curves were measured, injection of the helium-hydrocarbon mixture was accomplished by pushing the piston of the sampling valve from position A-a into position A-b (Figure 3). After the helium-hydrocarbon mixture from the sample loop was flushed with the carrier gas (helium) into the column, the piston was returned again into position A-a. Two sizes (0.25 and 1.0 ml.) of sample loops were used.

The measurement of the breakthrough curves was started by replacing the stream of helium, flowing at the beginning through the column, by the stream of helium-hydrocarbon mixture. The positions of the six-way valve initially and afterwards (B-a and B-b) are shown in Figure 3. In order to prevent changes in flow rate of the helium-hydrocarbon mixture after switching the sampling valve, the pressure in the feed line was adjusted by means of the needle valve (Figure 2) to the value of the carrier gas pressure at the bed inlet. However, this pressure was only a few millimeters of mercury higher than the pressure at the outlet of the column.

The columns (containing silica gel) were made of copper tubing. For particle size $R = 0.11$ mm., the column was ¼ in. O.D. and 30.1 cm. long (cross-sectional area 0.189 sq. cm.). For particle sizes $R = 0.39$ and $R = 0.50$ mm., ⅜ in. O.D. tubing, 13.0 cm. long, was used (cross-sectional area 0.472 sq. cm.). The interparticle void fractions (external porosities) α, for these columns were calculated from the known volume of the column (determined with mercury), and the weight and apparent density of silica gel. For $R = 0.11$ mm., $R = 0.39$ mm., and $R = 0.50$, these external void fractions were 0.378, 0.360, and 0.340. The intraparticle void volumes per unit of interparticle voids $[\beta(1 - \alpha)/\alpha]$ were, respectively, 0.800, 0.864 and 0.945.

CALCULATIONS

Evaluation of Moments of the Chromatographic Curves

Because of the direct proportionality between the gas concentration and the deflection of the recorder connected with the ionization detector at the column outlet, it is possible to evaluate the moments using the observed deflection in place of concentration in Equations (28) and (29).

The integrals were evaluated numerically (IBM 7044 computer) from the chromatographic curves using Simpson's rule.

Predicted Breakthrough Curves

Predicted breakthrough curves from Equations (9) to (20) are based on evaluation of the infinite integral, $\int_0^\infty (1/y) \exp [A_1(y)] \sin [A_2(y)]dy$, for proper values of the dimensionless parameters A, D, E and for definite values of the dimensionless time, τ. Since the integrand converges to zero as y increases, it was possible to replace

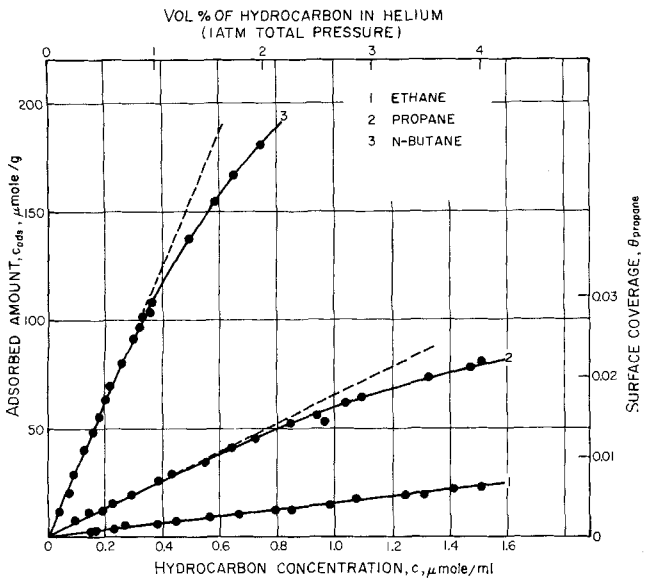

Fig. 4. Equilibrium of hydrocarbons on silica gel at 50°C. (Dashed lines represent linear isotherms obtained by chromatography, circles and solid lines are for dynamic adsorption method).

the improper upper limit by a finite one (y_{end}), chosen so that $(1/y_{end})\exp[A_1(y_{end})] \leq 5 \times 10^{-6}$. The integral was then evaluated numerically using Simpson's rule. A program was written which automatically changed the integration step (Δy) as long as the accuracy of the value of the relative concentration c/c_0 was better than 5×10^{-4}. The numerical work was carried out on the IBM 7044 computer.

EQUILIBRIUM ADSORPTION RESULTS

The low pressure adsorption isotherms of the three hydrocarbons are shown in Figure 4. Ethane exhibits a linear isotherm over the whole concentration range, while the curves for propane and *n*-butane have a linear portion only up to gas concentrations equivalent to 2 and 1% (by volume at 1 atm. total pressure). The degree of coverage of the silica gel surface was calculated for propane (θ_{prop}) using the value (30.3 sq. Å) recommended by Taylor and Atkins (9) for the area occupied by a propane molecule. From the isotherms it is evident that the linear region extends only over a few percent of monolayer coverage. The adsorption equilibrium constants, K_A, determined from the linear region are summarized in Table 1. At 50°C. the adsorption coefficient of propane is 4.5 times larger than that for ethane, while K_A for *n*-butane is in turn 4.8 times larger than the propane coefficient. Hence, for the substances studied the addition of a methylene group to a normal paraffin molecule causes nearly the same relative increase in adsorption coefficient.

TABLE 1. ADSORPTION COEFFICIENTS ON SILICA GEL AT 50°C

Hydrocarbon	Adsorption coefficient, K_A, (ml./g. SiO_2) From equilibrium adsorption measurements	From evaluation of chromatographic peaks
ethane	14.5	14.6
propane	63	65.4
n-butane	308	311

GAS-SOLID CHROMATOGRAPHY

A necessary condition for the theory of chromatography and breakthrough curves utilized in this paper is the linearity of the adsorption isotherm. For nonlinear isotherms the moments of the chromatographic curves should depend on the concentration in the injected pulse (*10*). However, it is expected that the concentration independence of the moments will extend somewhat beyond the concentrations for which the equilibrium adsorption is linear. This is because the concentration of the pulse travelling through the column rapidly decreases (*11*). During a substantial fraction of the time the pulse spends in the column, the concentration is far lower than it was at injection. This is confirmed in Figure 5, which shows that the first absolute moment, as well as the second central moment, of the chromatographic curves are independent of the concentration in the injected pulse up to concentrations higher than expected from the adsorption isotherms (Figure 4). Thus it should be possible to use pulses of ethane and propane containing up to 4% (vol.) of hydrocarbon, and pulses of *n*-butane with as much as 2%. However, in the subsequent work the concentrations used were 1.0, 1.0 and 0.5% for ethane, propane, and *n*-butane, respectively. Figure 5 also shows the degree of reproducibility of the first absolute moment and second central moment.

First Absolute Moments (Equilibrium Constants)

From Equations (31) and (34) it follows that

$$\frac{\Delta\mu_1 - \frac{t_{oA}}{2}}{\frac{1-\alpha}{\alpha}\beta} = \frac{\rho_p K_A}{\beta}\left(\frac{z}{v}\right) \tag{37}$$

where

$$\Delta\mu_1' = \mu_1' - (\mu_1')_{inert} \tag{38}$$

The first absolute moment for a nonadsorbable (inert) substance is given by Equation (31) with $K_A = 0$ and $t_{oA} = 0$. Hence

$$(\mu_1')_{inert} = \left(1 + \frac{1-\alpha}{\alpha}\beta\right)\frac{z}{v} \tag{39}$$

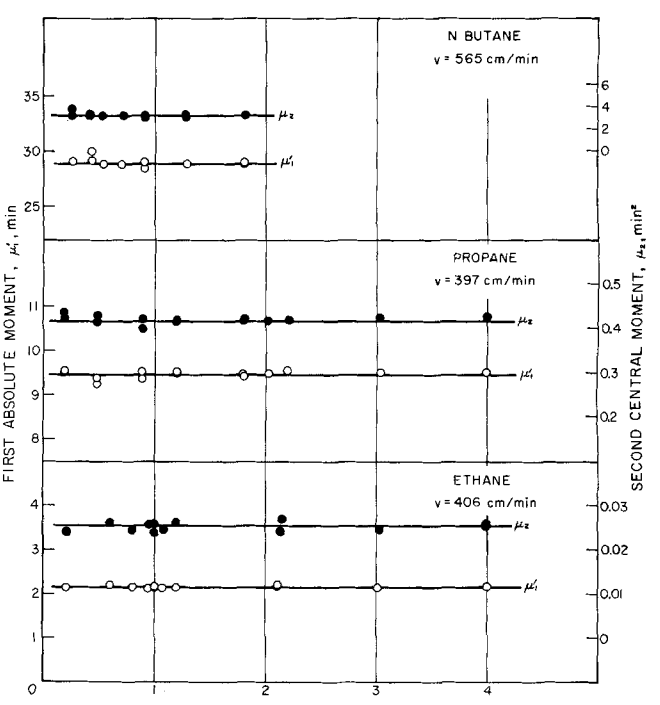

Fig. 5. Effect of hydrocarbon concentration on first and second moments at 50°C. (Column length 30.1 cm., particle size, R = 0.11 mm., sample size 0.25 ml.).

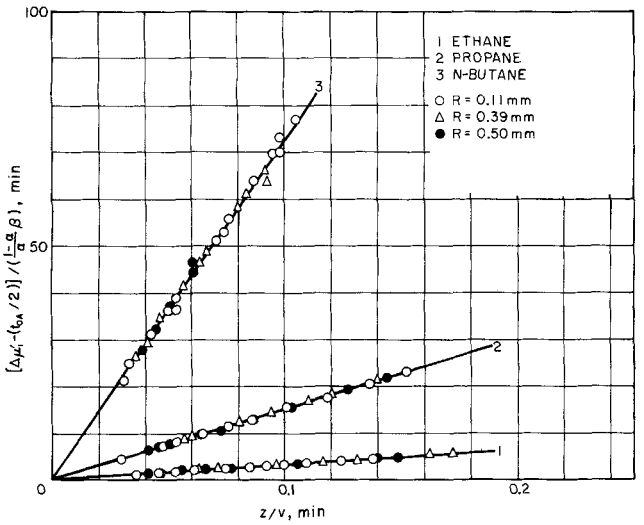

Fig. 6. Chromatography of hydrocarbons on silica gel (50°C.). (Dependence of the reduced first absolute moment on z/v).

It was necessary to calculate $(\mu_1')_{\text{inert}}$ in this way rather than measure it experimentally because the flame ionization detector did not respond to inert gases.

According to Equation (37) a plot of the reduced moment (the left member of the equation) vs. z/v should be a straight line through the origin. Furthermore, data for different sizes of silica gel particles should fall on the same line. Such a plot of the moments obtained from the chromatographic curves for three particle sizes is given in Figure 6 for the various hydrocarbons. It is apparent that the linearity requirement is fulfilled. The values of K_A determined from the slopes of the lines and Equation (37) are given in Table 1. The agreement between these K_A values and those determined from direct equilibrium measurements is good; the difference is about 1% for ethane and *n*-butane, and 3% for propane.

Second Central Moments

Equations (32), (34), and (35) relate the second central moment, μ_2, of the chromatographic peak at the column outlet to the width of the injected pulse (t_{oA}), the parameters which characterize the column and the adsorbent (z, α, β, ρ_p, R), the constants which describe the adsorption (K_A, k_{ads}), and the diffusional transports coefficients (D_c, k_f). Furthermore μ_2 is dependent on the velocity of the carrier gas. For analyzing the experimental data, Equation (32) was transformed into the form

$$\frac{\mu_2 - \frac{t_{oA}^2}{12}}{2(z/v)} = \delta_a + \delta_i + \delta_e + \frac{E_A}{\alpha}(1+\delta_o)^2\frac{1}{v^2} \quad (40)$$

where

$$\delta_a = \left(\frac{1-\alpha}{\alpha}\beta\right)\left(\frac{\rho_p}{\beta}\right)\frac{K_A^2}{k_{\text{ads}}} \quad (41)$$

$$\delta_i = \delta_o\frac{R^2\beta}{15}\left(1+\frac{\rho_p}{\beta}K_A\right)\frac{1}{D_c} \quad (42)$$

$$\delta_e = \delta_o\frac{R^2\beta}{15}\left(1+\frac{\rho_p}{\beta}K_A\right)\frac{5}{k_f R} \quad (43)$$

$$\delta_a + \delta_i + \delta_e = \delta_1 \quad (44)$$

The mass transfer coefficient, k_f, in Equation (43) depends in general on the velocity and the diameter of the particles. In analogy to the correlation of the heat transfer coefficient for forced convection around a sphere, the following correlation for mass transport coefficients has

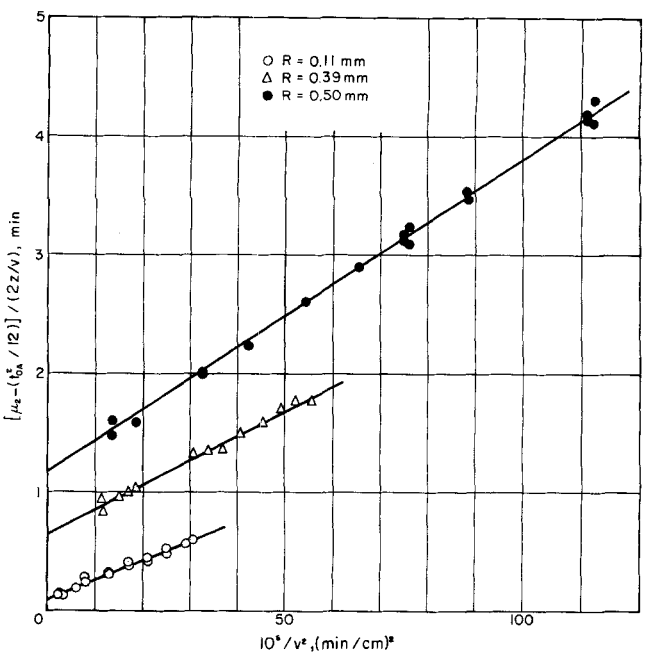

Fig. 7. Chromatography of ethane (50°C.). Dependence of $[\mu_2-(t^2_{oA}/12)]/2(z/v)$ on $1/v^2$.

been proposed (*12*):

$$N_{Nu_{AB}} = 2.0 + 0.60\,(N_{Re})^{1/2}(N_{Sc})^{1/3} \quad (45)$$

where the Nusselt number for mass transfer is defined as

$$N_{Nu_{AB}} = \frac{2R\,k_f}{\mathcal{D}_{AB}}$$

and the Reynolds and Schmidt numbers have their usual meaning

$$N_{Re} = \frac{2R\,v}{\nu}$$

$$N_{Sc} = \frac{\nu}{\mathcal{D}_{AB}}$$

Wakao (*13*) found this form of correlation satisfactory for data in packed beds down to very low values of the Reynolds number. At low Reynolds number Equation (45) shows that $N_{Nu_{AB}} = 2.0$ and the mass transfer coefficient is given by

$$k_f R = \mathcal{D}_{AB} \quad (46)$$

Accordingly, the mass transfer coefficient at low Reynolds numbers does not depend on velocity and is inversely

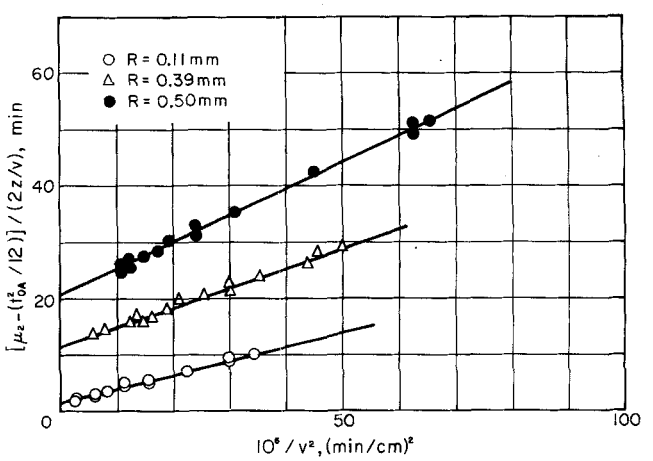

Fig. 8. Chromatography of propane (50°C.). Dependence of $[\mu_2-(t^2_{oA}/12)]/2(z/v)$ on $1/v^2$.

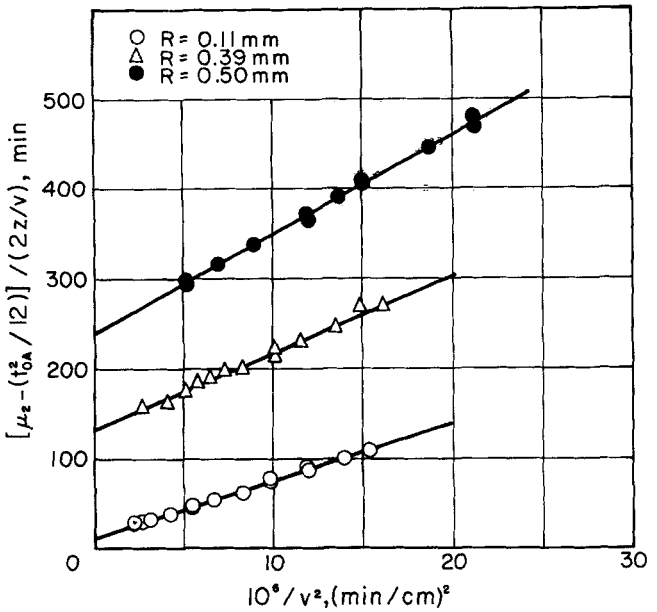

Fig. 9. Chromatography of *n*-butane (50°C.). Dependence of $[\mu_2-(t^2_{oA}/12)]/2(z/v)$ on $1/v^2$.

proportional to particle size. In all experiments reported here the Reynolds numbers were very low so that Equation (46) was always applicable. Substituting Equation (46) into Equation (43) suggests that none of the δ's depends on the velocity of the carrier gas. Therefore experimental data plotted as the left side of Equation (40) vs. $1/v^2$ should lie on a straight line with a slope of $E_A\ (1+\delta_o)^2/\alpha$ and intercept $(\delta_a+\delta_i+\delta_e)$. This is demonstrated in Figures 7, 8, and 9 which summarize the chromatographic data for ethane, propane, and *n*-butane for the three particle sizes.

If data were obtained for very high flow rates of the carrier gas (high N_{Re}) the mass transfer coefficient increases and the term δ_e decreases toward zero. In this case the experimental data should again fulfill the linear dependence between the left side of Equation (40) and $1/v^2$. The slope of such a straight line would again be $E_A\ (1+\delta_o)^2/\alpha$, but the intercept is now equal to $(\delta_a+\delta_i)$.

Axial Dispersion Coefficients

As K_A (and hence, δ_o) are known from the analysis of the first absolute moments, the axial dispersion coefficients, E_A, can be obtained from the slopes of the straight lines in Figures 7, 8, and 9. These coefficients are summarized in Table 2 together with the external tortuosity factors, q_{ext}, defined by the equation

$$E_A = \frac{\alpha}{q_{ext}}\mathcal{D}_{AB} \tag{47}$$

This definition supposes that the void structure of the bed of adsorbent can be represented by a parallel assembly of cylindrical capillaries of the same average diameter running in the direction of the gas flow. The tortuosity factor expresses the average length of the path followed by the flowing gas, relatively to the length of the bed. Equation (47) also is based upon the assumption that the axial dispersion is due only to molecular diffusion in the interparticle space. This is justified because at low Reynolds numbers the Peclet number is proportional to the Reynolds number.

TABLE 2. AXIAL DISPERSION COEFFICIENTS (50°C.)

	Particle radius (mm.)	Hydrocarbon: ethane	propane	*n*-butane	
	0.11	0.123	0.103	0.117	
E_A, sq.cm./sec.	0.39	0.127	0.117	0.123	
	0.50	0.130	0.125	0.130	
$\mathcal{D}_{AB}$* sq.cm./sec.		0.590	0.483	0.462	
					avg.
	0.11	1.81	1.77	1.49	1.69
q_{ext}	0.39	1.67	1.49	1.35	1.50
	0.50	1.55	1.31	1.21	1.36

* The molecular diffusivities, $\mathcal{D}_{AB}$, were calculated from Hirschfelder's equation (*12*). The potential constants, ϵ/k and σ, for ethane and propane were those published by Bird, Stewart and Lightfoot (*12*); potential constants for *n*-butane were taken from Reid and Sherwood (*16*).

According to this model, the external tortuosity factor for different hydrocarbons should be nearly the same, as long as the particle size of the adsorbent and the packing of the bed are the same. The data in Table 2 scatter somewhat but, in general, support this view. For each particle size the largest deviation of the tortuosity factors from the average value is approximately 10%. It also appears that the average value of q_{ext} decrease with increasing particle size, indicating that the path length is shorter for larger particle diameters. This is reasonable since beds formed from larger particles have larger interparticle void spaces. The difference in external void fraction, α, between the smallest (R = 0.11 mm.) and largest (R = 0.50 mm.) particles is about 11% while the difference in external tortuosity factors is about 20%.

Adsorption Rate Constant

Since k_f is given by Equation (46), it was possible to determine the adsorption rate constant k_{ads}, and the effective internal diffusion coefficient, D_c, for each particle size, from the intercepts in Figures 7 to 9. First the method of obtaining k_{ads} is described. Figure 10 is a plot of the intercepts in Figures 7 to 9, which according to Equation (44) are equal to δ_1 vs. R^2. Reference to Equa-

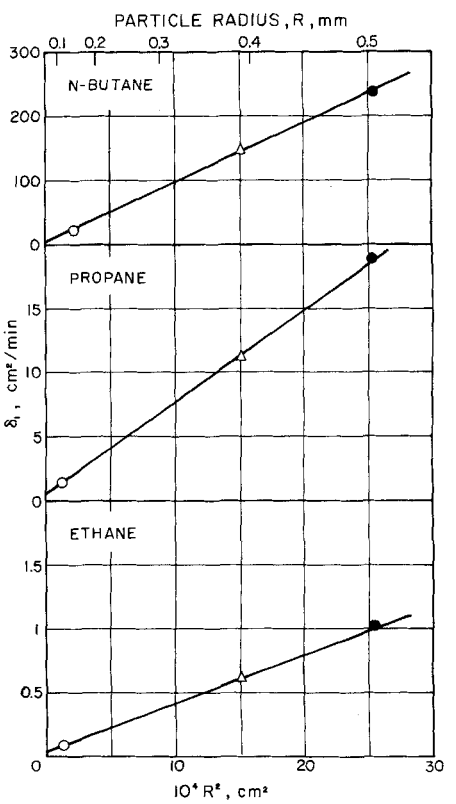

Fig. 10. Dependence of δ_1 on R^2.

tions (41) to (44), shows that such a plot should be a straight line with an intercept equal to δ_a. Values of δ_a established from the three curves in Figure 10 can be used in Equation (41) to determine k_{ads}. The results are as follows:

Substance	k_{ads} (50°C.) ml./g. SiO_2
ethane	167.
propane	255.
n-butane	1500.

The accuracy of these adsorption rate constants is uncertain due to the rapidity of the adsorption process on the silica gel surface. This results in a very small intercept, δ_a. However, k_{ads} does increase with molecular weight of adsorbent as would be expected.

Intraparticle Diffusivity

The slopes of the lines in Figure 10, according to Equations (42) and (43), are equal to $(\delta_i + \delta_e)/R^2$. Since k_f and K_A are known, δ_e can be determined and used with these slopes to establish values of δ_i. Then D_c is obtained from Equation (42). The effective diffusivities so determined are presented in Table 3. Since the pores in silica gel are very small, transport in the pore volume is by Knudsen diffusion. If the porous gel is represented by an assembly of parallel, cylindrical capillaries, the effective diffusivity can be used to define an internal tortuosity factor, q_{int}, according to the usual equation

$$D_c = \frac{\beta}{q_{int}} \mathcal{D}_k \qquad (48)$$

In this expression $\mathcal{D}_K$ is the Knudsen diffusivity evaluated, at $\bar{r} = 11$ Å., from the equation

$$\mathcal{D}_K = \frac{4}{3}\bar{r}\left(\frac{2R_gT}{\pi M}\right)^{1/2} \qquad (49)$$

The internal tortuosity factors so calculated are also given in Table 3.

TABLE 3. EFFECTIVE DIFFUSION COEFFICIENTS (50°C.)

	Ethane	Propane	*n*-Butane
$D_c \times 10^3$ (sq.cm./s)	1.41	1.54	2.93
$\mathcal{D}_K \times 10^3$ (sq.cm./s)	3.48	2.89	2.52
q_{int}	1.20	0.91	0.42

For a porous solid with only one maximum in the volume distribution of pore radii, as is the case for silica gel, Equation (54) should correlate diffusivities reasonably well; that is, q_{int} should be constant (*14*). The level of q_{int} should be greater than unity and presumably be of the order of 2 to 3. However, if another diffusional process exists, such as surface migration of the adsorbed molecules, the observed tortuosity would be decreased. Since the values given in Table 3 are much less than 2, it is indicated that surface diffusion is occurring and that it becomes more significant in changing adsorbates from ethane to *n*-butane. Its increase in significance with molecular weight of adsorbate is expected since the adsorbed concentration increases. The role of surface diffusion in these results is discussed in the subsequent paper (*15*). What is to be noted here is that the effective diffusivities in Table 3 are applicable for use in predicting breakthrough curves. This is because surface migration operates in a parallel manner with gaseous diffusion in the volume of the pores, regardless of the concentration change imposed as an initial condition at the entrance to the bed of adsorbent particles.

Discussion

The terms δ_a, δ_i, and δ_e can be visualized as increments to the total width of the chromatographic curve due to the resistances of the adsorption, internal diffusion, and external diffusion processes. Axial dispersion cannot be depicted in this way, because its significance changes with the rate of flow of the carrier gas. Ratios such as δ_a/δ_1, then show the relative importance of a particular process (when axial dispersion is not taken into the account). In Table 4 these ratios are shown for the largest and smallest particle sizes. It is clear, that for the largest particles ($R = 0.50$ mm.), intraparticle diffusion controls the overall process; the adsorption and external diffusion resistances combined contribute less than 4% of the total. The resistance of the adsorption process is lower for hydrocarbons with higher molecular weight while the converse is true for external diffusion. This is because the mass transfer coefficient is proportional to the molecular diffusivity, $\mathcal{D}_{AB}$, which is in turn inversely proportional to the molecular weight. For the smallest particles ($R = 0.11$ mm.) the contributions of the adsorption process and external diffusion are larger. However, intraparticle diffusion still plays the major role. As could be expected the resistance of the adsorption process is largest for ethane and lowest for *n*-butane.

TABLE 4. CONTRIBUTIONS (%) OF THE THREE RESISTANCES TO THE SECOND CENTRAL MOMENT OF THE CHROMATOGRAPHIC CURVE

	Ethane		Propane		*n*-Butane	
	$R =$ 0.11 mm.	$R =$ 0.50 mm.	$R =$ 0.11 mm.	$R =$ 0.50 mm.	$R =$ 0.11 mm.	$R =$ 0.50 mm.
Adsorption resistance*	44.5	4.0	37.7	3.0	16.0	1.0
Intraparticle diffusion resistance†	54.8	95.0	61.5	95.9	81.4	95.1
External diffusion resistance‡	0.7	1.0	0.8	1.1	2.6	3.1

* δ_a/δ_1
† δ_i/δ_1
‡ δ_e/δ_1

Particularly interesting is the minor part that the external diffusion process plays in all cases. It should be noted also that at higher flow rates k_f would increase, thus further decreasing the significance of mass transport to the external surface.

For the largest particles, the calculated values of the intraparticle diffusivity are not affected by neglecting the adsorption and external diffusion resistances. If these resistances are completely neglected, D_c for ethane becomes 1.37×10^{-3} sq.cm./sec. in comparison with 1.41×10^{-3} from Table 3. For *n*-butane the difference is even less, 2.92×10^{-3} vs. 2.93×10^{-3} sq.cm./sec. Serious errors would result if this procedure were applied to the smallest particles. When $R = 0.11$ mm., D_c for ethane is but 0.80×10^{-3} sq.cm./sec. and for *n*-butane, 2.35×10^{-3} sq.cm./sec.

While the effect of axial dispersion cannot be represented as an additive resistance, its relative importance can be evaluated at a given velocity from the ratio

$$\frac{(E_A/\alpha)(1+\delta_o)^2(1/v^2)}{\delta_1 + (E_A/\alpha)(1+\delta_o)^2(1/v^2)}$$

This ratio can be evaluated by referring to Figures 7, 8, and 9 for ethane, propane, and *n*-butane. The value of δ_1 is given by the intercept and $(E_A/\alpha)(1+\delta_o)^2(1/v^2)$ is given by the verticle distance between δ_1 and the point

Table 5. Key for Figure 11, Comparison of Calculated and Experimental Breakthrough Curves

Curve	Hydrocarbon	R^* (mm.)	t_o (min.) Eq. (17)	Parameters values for calculated curves: Internal diffusion D	External diffusion E	Adsorption A
1	ethane	0.50	1.36	3.24	2.39×10^{-3}	340.0
2	ethane	0.11	2.14	97.3	2.39×10^{-3}	17.2
3	propane	0.50	9.56	4.86	3.19×10^{-3}	475.0
4	propane	0.11	6.83	68.1	3.19×10^{-3}	24.1
5	*n*-butane	0.50	44.6	8.1	6.36×10^{-3}	1468.0
6	*n*-butane	0.11	38.4	115.7	6.36×10^{-3}	74.5

* Lengths of the columns, z = 30.1 cm., 13.0 cm., 13.0 cm. for particles of R = 0.11 mm., R = 0.39 mm., R = 0.50 mm. respectively.

on the curve corresponding to a particular velocity. It is apparent from these plots that the value of the ratio can vary from almost unity at a very low velocity down to zero at a velocity approaching infinity. In the intermediate range at which our experimental work was carried out, values of this ratio would be finite, indicating that axial diffusion was important. In other words, erroneous results would have been obtained for such parameters as the intraparticle diffusivity had axial dispersion been neglected. Only at very high velocities would it be possible to neglect this contribution to the shape of the chromatographic wave.

BREAKTHROUGH CURVES

The rate constants k_{ads} and D_c determined from analysis of chromatographic data can now be used to predict breakthrough curves by using Equations (9) to (20). To illustrate the results, Figure 11 shows such predicted curves and the experimental data points for the largest and smallest particle sizes. The numerical values of the parameters **D**, **E**, and **A** for the predicted curves were determined from Equations (18) to (20) and are given in Table 5. Also tabulated there are the values of t_o, calculated from Equation (17), which were used to determine the dimensionless time scale, τ. The steeper curves are for R = 0.11 mm. while the flatter curves are for R = 0.50 mm.

The agreement between the experimental data and predicted curves is excellent. This is perhaps surprising since the prediction method neglects axial dispersion and in the previous section it was shown that axial dispersion influences the chromatographic wave. However, it is possible that axial disperison has more influence in chromatographic measurements than on breakthrough curves. This is supported by the work of Babcock and colleagues (*17*) who recently have analyzed the behavior of a packed bed, generalizing the earlier solutions (*1* to *3*) to include axial dispersion. Their results predict temperature breakthrough curves in response to a step-function input of thermal energy. However, it is possible from their results to infer conclusions about concentration breakthrough curves. They have shown that the term involving axial dispersion depends on the intraparticle diffusion resistance (R^2/D_c). Thus the effect of axial dispersion can be unimportant when intraparticle diffusion resistance is large. Such coupling of these two effects does not occur in the analysis of chromatographic curves [see Equation (32)].

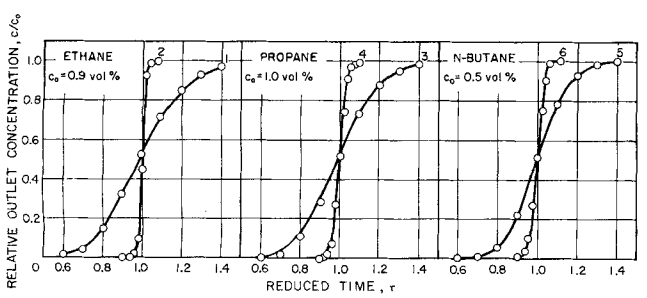

Fig. 11. Comparison of calculated and experimental breakthrough curves (50°C.) (Solid lines denote experimental curves; points are calculated).

It was shown that for R = 0.50 mm. neglecting adsorption and external mass transfer resistances had but a small effect on the value of D_c obtained chromatographically. Hence, breakthrough curves based upon neglecting the same resistances should have a good approximation to experimental breakthrough curves. This is illustrated in Table 6 which gives predicted concentration ratios for propane when all three resistances are considered, and when the adsorption resistance is neglected ($\mathbf{A} \to \infty$), the external diffusion resistance is neglected ($\mathbf{E} \to 0$), and when both resistances are neglected. In all cases the c/c_o results are nearly identical.

Table 6. Breakthrough Calculations for Propane at 50°C.
(R = 0.50 mm., v = 2.88 cm./sec.)

Reduced time, τ	Relative concentration, c/c_o (%): D = 4.86, E = 3.19 × 10^{-3}, A = 475.0	D = 4.86, E = 3.19 × 10^{-3}, (A → ∞)	D = 4.86, (E → 0), (A → ∞)	D = 4.80, (E → 0), (A → ∞)
0.80	10.4	10.9	10.7	10.8
0.84	16.5	16.9	16.7	16.9
0.88	24.1	24.5	24.3	24.4
0.92	33.0	33.2	33.1	33.2
0.96	42.6	42.7	42.7	42.7
1.00	52.4	52.4	52.4	52.4
1.04	61.7	61.6	61.7	61.6
1.08	70.3	70.0	70.1	70.0
1.12	77.6	77.3	77.4	77.3
1.16	83.6	83.3	83.5	83.3
1.20	88.4	88.1	88.3	88.1

CONCLUSIONS

A method has been presented for obtaining adsorption rate constants for adsorption by analysis of chromatographic data. Further, it is possible to predict breakthrough curves using the adsorption equilibrium constants, adsorption rate constants, and effective intraparticle diffusivities obtained from the chromatographic curves. In this paper the first absolute and second central moments were utilized. This required measuring chromatographic curves for different carrier gas velocities and for different particle sizes of adsorbent. However, when the resistance of the adsorption process on the surface

need not be considered, it is sufficient to vary only the carrier gas velocity. The intraparticle diffusion coefficients which result from such treatment are accurate enough for the prediction of the breakthrough curves.

In principle there is another way to obtain the necessary constants which requires even less experimental measurements. It is based on analysis of the first, second, and third moments of the chromatographic wave, or more generally, on the analysis of any three moments. Unfortunately, the calculation of the third and higher moments necessitates very accurate experimental data. In the calculation of the higher moments, serious troubles arise from the uncertainty of the exact position of the tails of the chromatographic curves. A relatively minor change in the tail concentration is enlarged by multiplication by the third (or higher) power of time. This uncertainty in the higher moments can be overcome when the same measurement is repeated several times and the results are treated statistically, but then there is no reduction in extent of experimental measurements. When more accurate concentration detection devices are developed, the analysis of higher moments may be advantageous.

ACKNOWLEDGMENT

The financial assistance provided for this study by the National Science Foundation through Grant No. GP-2990, and the support of the Computer Center of the University of California, Davis, through National Institutes of Health Grant No. Fr-00009, are gratefully acknowledged.

NOTATION

$A_1(y), A_2(y)$ = functions given by Equation (10) and (11)
$\mathbf{A}$ = adsorption parameter, Equation (20)
c = concentration of the adsorbable gas in the interparticle space, mole/ml.
c_i = concentration of the adsorbable gas in the pore space, mole/ml.
c_{ads} = concentration of the adsorbed gas per unit weight of adsorbent, mole/g.
c_o = concentration of the adsorbable gas in the input concentration function, mole/ml.
$\mathbf{D}$ = intraparticle-diffusion parameter, Equation (18)
D_c = effective intraparticle diffusion coefficient defined as the ratio of the diffusional flux through unit area of the geometrical surface of the particle to the negative of the intraparticle concentration gradient, sq.cm./sec.
$\mathcal{D}_{AB}$ = binary molecular diffusivity, sq.cm./sec.
$\mathcal{D}_K$ = Knudsen diffusivity, sq.cm./sec.
$\mathbf{E}$ = external diffusion parameter, Equation (19)
E_A = effective axial dispersion coefficient, defined as the ratio of the axial diffusional flux through unit area of the total cross section of the column to the negative of the interparticle concentration gradient sq.cm./sec.
$h(p)$ = function given by Equation (25)
k_{ads} = adsorption rate constant, defined by Equation (3), ml/g.sec.
k_f = mass transfer coefficient defined by Equation (4), cm./sec.
K_A = adsorption equilibrium constant (adsorption coefficient), defined as $(c_{ads}/c)_{equil}$, ml./g.
m_n $(n = 0,1,2,..)$ = integrals, Equation (28)
M = molecular weight of the diffusing substance, g./mole
$N_{Nu_{AB}}$ = Nusselt number for mass transfer, Equation (45)
N_{Re}, N_{Sc} = Reynolds number, Schmidt number
p = variable in the Laplace-Carson transformation
q_{int}, q_{ext} = tortuosity factors for intraparticle diffusion and for axial dispersions, Equations (47), (48)
r = length coordinate in the spherical particle of absorbent, measured from the center of particle, cm
$\bar{r}$ = average radius of the pores, cm
R = radius of the spherical particle of adsorbent, cm.
R_g = gas constant
s = Laplace-Carson transform of $c(z,t)$, Equations (22) and (23)
t = time, sec.
t_o = time necessary for saturation of the adsorbent in the bed under conditions of no resistance, Equation (17), sec.
$t_{oA}, (t_o)_{inert}$ = time of duration of the injection of the absorbable or inert gas in chromatography, sec.
T = absolute temperature, °K
v = linear velocity of the carrier gas in the interparticle space, cm./min.
w = deflection of the recorder pen
y = integration variable, Equation (9)
z = length coordinate of the bed of adsorbent, measured from the inlet side, cm.

Greek Letters

α = interparticle void fraction in the absorbent bed
β = intraparticle void fraction (internal porosity) of the adsorbent
γ = defined by Equation (24)
$\delta_0, \delta_1, \delta_2, \delta_a, \delta_b, \delta_e$ = expressions defined by Equations (34), (35), (36), and (41) to (43)
ω_1, ω_2 = functions defined by Equation (12), (13)
ϕ_1, ϕ_2 = functions defined by Equation (14), (15)
λ = expression defined by Equation (26)
μ_n', μ_n = nth absolute and central moment of the chromatographic curve, respectively, Equations (27), (29)
$(\mu_1')_{inert}$ = first absolute moment for the nonadsorbable gas calculated from Equation (39)
ρ_p = apparent particle density, g./ml.
τ = reduced time defined by Equation (16)
ν = kinematic viscosity.

LITERATURE CITED

1. Masamune, S., and J. M. Smith, *AIChE. J.*, **11**, 34 (1965).
2. ———, *Ind. Eng. Chem. Fundamentals*, **3**, 179 (1964).
3. Rosen, J. B., *J. Phys. Chem.*, **20**, 387 (1952).
4. Kubin, M. *Collection Czechoslov. Chem. Commun.*, **30**, 1104 (1965).
5. Ibid., 2900 (1965).
6. Kucera, E., *J. Chromatography*, **19**, 237 (1965).
7. Ditkin, V. A., and P. I. Kuznetsov, "Spravochnik po operacionnomu ischisleniju," p. 140, Gostechizdat, Moscow, (1951).
8. Masamune, S., and J. M. Smith, *AIChE J.*, **11**, 41 (1965).
9. Taylor, G. L., and J. H. Atkins, *J. Phys. Chem.*, **70**, 1051 (1966).
10. Houghton, G., *ibid.*, **67**, 84 (1963).
11. Eberly, P. E. Jr., and E. H. Spencer, *Trans. Faraday Soc.*, **57**, 289 (1961).
12. Bird, R. B., W. E. Stewart, and E. N. Lightfoot, "Transport Phenomena," John Wiley, New York (1960).
13. Wakao, N., T. Oshima, and S. Yagi, *Kagaku Kogaku*, **22**, 780 (1958); Chem. Abstr., 2702g (1959).
14. Satterfield, C. N., and T. K. Sherwood, "The Role of Diffusion in Catalysis," Addison-Wesley, Reading, Mass. (1963).
15. Schneider, P., and J. M. Smith, *AIChE J.*, (1968).
16. Reid, R. C., and T. K. Sherwood, "Properties of Gases and Liquids," McGraw-Hill, New York, (1958).
17. Babcock, R. E., D. W. Green, and R. H. Perry, *AIChE J.*, **12**, 922 (1966).

Manuscript received January 24, 1967; revision received June 5, 1967; paper accepted July 21, 1967.